Engineering Structures 206 (2020) 110152

Contents lists available at ScienceDirect

Engineering Structures

journal homepage: www.elsevier.com/locate/engstruct

Fragility analysis of high CFRDs subjected to mainshock-aftershock sequences based on plastic failure

Rui Pang[a,b], Bin Xu[a,b], Yang Zhou[a,b,*], Xu Zhang[a], Xingliang Wang[a]

[a] School of Hydraulic Engineering, Faculty of Infrastructure Engineering, Dalian University of Technology, Dalian 116024, China
[b] State Key Laboratory of Coastal and Offshore Engineering, Dalian University of Technology, Dalian 116024, China

ARTICLE INFO

Keywords:
High CFRD
Mainshock-aftershock sequences
MSA
Engineering demand parameter
Fragility

ABSTRACT

Numerous earthquake disasters have demonstrated that secondary damage to structures induced by aftershocks may seriously threaten the seismic safety of structures since the mainshock may have already weakened structural integrity. This paper investigates the fragility of a 200-m high concrete face rockfill dam (CFRD) subjected to mainshock-aftershock sequences based on multiple stripes analysis (MSA). A modified generalized plasticity model and a plastic-damage model are used to describe the nonlinearity of the rockfills and the concrete face slabs, respectively. A series of nonlinear dynamic time history analyses for the CFRD under mainshock-aftershock sequences with different intensity combinations are conducted. The analysis focuses on the deformations, the shear strains and the damage index (DI) of the face slabs. According to the analysis results, the vertical deformation is the best indicator of the cumulative damage inflicted by aftershocks on the high CFRD. Then, considering the importance of face slab damage to the integrity and performance of the CFRD, the influences of aftershocks on the probability of the CFRD reaching a specific limit state are discussed based on vertical deformation and DI. The results reveal that aftershocks can significantly increase the fragility of the CFRD when it has been damaged by mainshocks.

1. Introduction

A large number of historical earthquake data reveal the earthquakes typically are comprised of a sequence of shocks, a mainshock followed by multiple aftershocks [1–4]. During earthquake events, over a period of time (minutes, hours or days) after a mainshock, one or more aftershocks may occur. The Wenchuan earthquake with a mainshock measured M_w 8.0 on May 12, 2008, is a typical example of mainshock-aftershock sequences. During this earthquake, 42,719 aftershocks occurred between May 12 and November 6 [2]. The structure can enter the plastic stage after undergoing a large mainshock upon which the strength and stiffness of the structure can deteriorate to a certain degree. The following aftershocks can cause serious cumulative damage to the mainshock-damaged structure and even cause the complete collapse of the structure. Unfortunately, current seismic design codes in China only focus on resisting the mainshock of an earthquake and do not take potential aftershocks into account [5]. Therefore, it is of great significance to investigate the seismic performance of structures under mainshock-aftershock sequences.

Researchers all over the world have studied the influence of mainshock-aftershock sequences on the seismic performance of dams from multiple aspects. Alliard et al. [6] evaluated the seismic safety of gravity dams under mainshock-aftershock sequences when the dams suffered from reduced drainage efficiency. They found that the aftershock response was especially sensitive to the dimensions of the drainage system and other model parameters. An investigation carried out by Zhang et al. [7] discovered that aftershocks had a significant effect on the cumulative damage of the concrete gravity dams. Wang et al. [8] used 20 as-recorded mainshock-aftershock seismic sequences to evaluate the effects of aftershocks on concrete gravity dam-reservoir-foundation systems. The results indicated that the aftershocks caused more damage to an undamaged dam than to a dam which was already damaged by the mainshock. Furthermore, repeated ground motions tended to cause an underestimation of the level of seismic damage demand. Pang et al. [9] evaluated the seismic performance of CFRDs under mainshock-aftershock sequences using dam deformation, dam slope stability and face slab safety as metrics. The research concluded that CFRDs can experience additional damage due to aftershocks. In the

* Corresponding author at: School of Civil Engineering and State Key Laboratory of Coastal and Offshore Engineering, Dalian University of Technology (DUT), No. 2 Linggong Road, High-tech Zone, Dalian 116024, China.
E-mail addresses: pangrui@dlut.edu.cn (R. Pang), xubin@dlut.edu.cn (B. Xu), zhouy@dlut.edu.cn (Y. Zhou), zxkingdl@mail.dlut.edu.cn (X. Zhang), wxlyxx666@mail.dlut.edu.cn (X. Wang).

https://doi.org/10.1016/j.engstruct.2019.110152
Received 27 August 2019; Received in revised form 25 December 2019; Accepted 25 December 2019
Available online 02 January 2020

above studies, mainshock-aftershock sequences with different construction methods were adopted and seismic performance analyses of dams under sequence earthquakes were carried out. However, the above research efforts focused on the response characteristics of structures under seismic sequences based on deterministic analysis, and the uncertainties of ground motion were not taken into account.

Fragility analysis is a method to obtain the failure probability of structures subjected to specific earthquake intensity and it can solve the problem of ground motion uncertainty from the perspective of probability. Many scholars have applied fragility analysis to the seismic performance evaluation of some structures and it is also widely used in the field of dam engineering. Hariri-Ardebili et al. [10–12] conducted a comprehensive fragility analysis of concrete dams. They proposed a probabilistic seismic demand model with an optimal intensity measure (IM) for concrete gravity dams and evaluated the seismic fragility of the Pine Flat gravity dam through cloud analysis. The fragility analysis framework was presented within the scope of performance-based earthquake engineering analysis for concrete dams. Wang et al. [13] investigated the seismic fragility and performed damage analyses for arch dams with random material parameters and ground motions. Recently, Gasser et al. [14,15] contributed considerably to the application of the fragility analysis method for arch dams. In their studies, the randomness of parameters was fully considered, and for the first time, the water level variability was accounted for in a probabilistic seismic analysis of a dam. In addition to the above mentioned, there have been many other research efforts dedicated towards improved understanding of dam fragility [16–21]. The literature shows that the fragility analysis method has been widely used for gravity dams and arch dams. However, the fragility analysis of earth rock dams subjected to mainshock-aftershock sequences, especially for high CFRDs, has not been studied. At the same time, numerous high CFRDs are under construction or have been already built in the earthquake-prone regions of China [22,23]. Although the seismic performance of high CFRDs has been discussed by many researchers [24–28], either only a single earthquake was considered or a fragility analysis was not carried out in their research. Considering the above limited research progress, it is necessary to analyze the fragility of high CFRDs under the action of mainshock-aftershock sequences.

This paper examines the effects of aftershocks on the fragility of a 200-m high CFRD that has been damaged by mainshocks. Fifteen as-recorded mainshock-aftershock sequences are selected from PEER [29] and COSMOS [30] to study the plastic failure of high CFRD subjected to mainshock-aftershock sequences. Based on a series of nonlinear dynamic time history analyses, an EDP (Engineering Damage Parameter), which can best reflect the cumulative damage effect of aftershocks on the dam, is selected among displacement, shear strain and DI [24]. It is noteworthy that the relative intensity of aftershock [31] (i.e. ratio of aftershock intensity to mainshock intensity) is introduced as a parameter to quantify the intensity of aftershock. In light of the above research, the fragility of the CFRD under seismic sequences is obtained via MSA. The impact of aftershocks on the fragility of the CFRD can be seen through the analyses.

2. Fragility analysis method

At present, most scholars [24,32] use a lognormal cumulative distribution function to describe fragility:

$$P_R(C|IM = X) = \Phi\left[\frac{\ln(X/\theta)}{\sigma}\right] \tag{1}$$

where $P_R(C|IM = X)$ is the probability of making the structure reach a certain performance level under a ground motion $IM = X$; $\Phi()$ is the standard normal cumulative distribution function; IM is the intensity measure of the ground motion (peak ground acceleration (PGA) is used in this paper); θ, σ are respectively the logarithmic mean and logarithmic standard deviation of the ground motion intensity factors needed to reach a certain performance level, and are obtained by maximizing the likelihood function.

The maximum likelihood estimates for θ and σ are as follows [32]:

$$\begin{pmatrix}\hat{\theta}\\ \hat{\sigma}\end{pmatrix} = \arg\max \sum_{j=1}^{m}\left\{\ln\binom{n_j}{z_j} + z_j \ln\Phi\left(\frac{\ln(x_j/\theta)}{\sigma}\right) + (n_j - z_j)\ln\left[1 - \Phi\left(\frac{\ln(x_j/\theta)}{\sigma}\right)\right]\right\} \tag{2}$$

The fragility functions obtained from Eq. (2) differ because the least-squares method ignores the fundamental property of the data: the variance of the observed fractions of collapse is nonconstant and is in violation of the requirements of least squares fitting [32]. The relative intensity $\nabla PGA = PGA_{as}/PGA_{ms}$ represents the different intensity combinations of mainshock-aftershock sequences.

3. Model description and ground motions

3.1. Finite element mesh of the CFRD

In this paper, a 200-m high CFRD is used as the research case. Its two-dimensional finite element model is described in Fig. 1. The detailed dimensions and parameters are as follows: The upstream and downstream dam slopes are 1:1.4 and 1:1.5, respectively. The width of the dam crest is 13 m. The upstream of the dam has cushion zones with a horizontal width of 2.4 m and transition zones with a horizontal width of 3.6 m. The thickness of the face-slabs is 0.99 m. An added mass [33] is used to simulate the hydrodynamic pressure (height of impounded water is 180 m) of the concrete face slabs. The interface between the face slabs and cushions are simulated with an asymmetric interface proposed by Qu et al. [34] based on the Goodman element. A viscous-spring boundary combined with an equivalent nodal loading proposed by Liu et al. [35], is used to simulate the interaction between finite fields and infinite domains. Ground motions were input in the form the equivalent nodal loading at the boundaries of the model.

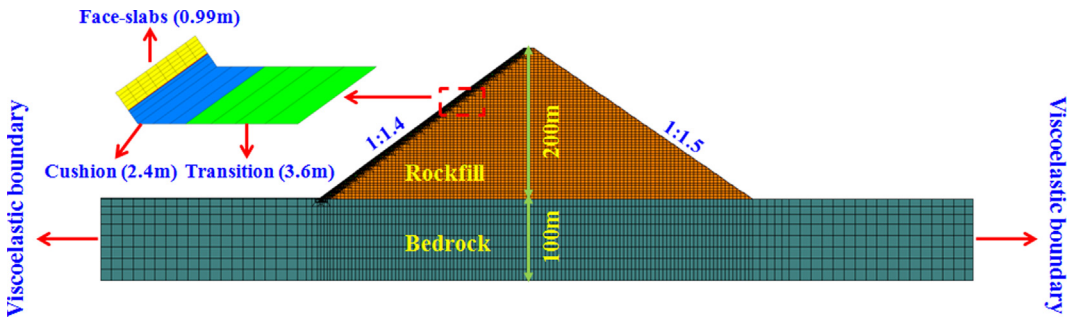

Fig. 1. 2-D Finite element mesh of the 200-m high CFRD.

3.2. Model parameters

In this paper, the plastic-damage model proposed by Lee and Fenves [36,37] is introduced to describe the damage behaviour of concrete face slabs, and this model was used to simulate the damage characteristics of concrete face slabs successfully in prior works [26,38]. The stress-strain relationship in the model is given by

$$\sigma = (1-\mathrm{d})\bar{\sigma} = (1-\mathrm{d})\mathrm{E}_0(\varepsilon - \varepsilon^{\mathrm{p}}) \tag{3}$$

where $\bar{\sigma}$ is the effective stress, E_0 is the initial elastic modulus, ϵ is the overall strain, ϵ_p is the plastic strain, and $d(0 < d < 1)$ is the damage factor.

According to Pang et al. [24], the DI is used to describe the degree of damage in the concrete face slabs, which is defined as:

$$DI = \alpha \cdot \frac{\sum_{i=1}^{n}\left(d_i \cdot S_i \cdot \frac{0.9H - h_i}{0.25H}\right)}{\sum_{i=1}^{n}\left(S_i \cdot \frac{0.9H - h_i}{0.25H}\right)} \tag{4}$$

where d_i is the damage factor of the ith element of the face slabs, n is the number of face-slab elements in 0.4–0.9H, S_i is the area of the ith element of the face slabs, h_i is the height of the ith element located between the center of the face slabs and the bottom of the face slabs, DI is the damage index of the face slabs, and α is the influence coefficient.

The dissipation energy density is related to the characteristic length of the width of the breaking zone. Therefore, an appropriate mesh size is the key to ensure that the finite element analysis results are more accurate. The determination of mesh size is usually an important step that is discussed in similar types of research [39]. For this purpose, different mesh sizes are applied to the same model in order to investigate the effect of mesh size on the accuracy. Fig. 2 shows the finite element meshes included for mesh size sensitivity test, and $G_t = 12.3$ N/m, $G_c = 1750$ N/m, $f_t = 3.48$ MPa and $f_c = 15.6$ MPa. Fig. 3 shows the stress-strain curves of these simulations. Following expectations, the smaller of the mesh size, the gentler the softening curve becomes after damage.

The plastic-damage model parameters, which are used to analyze the plastic-damage behaviour of the concrete face slabs, are shown in Table 1. The parameters of the rockfill materials and the interface between the concrete face slabs and cushion are listed in Tables 2 and 3, respectively, and they are used to simulate the Zipingpu CFRD during the Wenchuan earthquake [40,41]. Fig. 4 presents elastoplastic models of the rockfills in the paper.

3.3. Ground motions

Fifteen as-recorded seismic sequences in this study are all from PEER [29] and COSMOS [30]. Although mainshocks are typically followed by more than one aftershock in real earthquakes, in this study, only one aftershock is considered for each selected earthquake sequence for the sake of convenience. The mainshocks and the aftershocks have magnitudes greater than 5. The peak acceleration of the mainshocks is greater than 0.2 g and that of the aftershocks is greater than 0.1 g. The mainshock and the aftershock of each seismic sequence are chosen from the same station. In order to avoid the influence of soil-structure interactions, these stations are chosen so that they are in free-field sites or in low height buildings [42]. In addition, to ensure that the structures have sufficient time to achieve equilibrium prior to subsequent ground motions, a 10-s interval is set between two seismic events for each seismic sequence. Detailed features of selected seismic sequences are listed in Table 4.

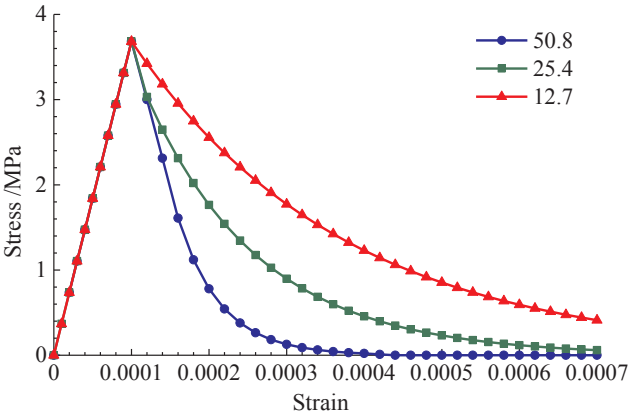

Fig. 3. Stress-strain curves for different meshes.

Table 1
Parameters of concrete face slab.

ρ/[kg/m^3]	E/[Pa]	f_t/[MPa]	f_c/[MPa]	G_t/[N/m]	Gc/[N/m]	L/[mm]	μ
2400	3.1e10	3.48	27.6	300	5690	43.0	0.167

Table 2
Parameters of rockfill materials.

ρ/[kg/m^3]	G_0	K_0	M_g	M_f	α_f	α_g	H_0	H_{U0}
2160	1000	1400	1.80	1.38	0.45	0.40	1800	3000
m_s	m_v	m_l	m_u	r_d	γ_{DM}	γ_u	β_0	β_1
0.50	0.50	0.20	0.20	105	50	4	35	0.022

Table 3
Parameters of interface material.

D_{s0}/[kPa]	D_{n0}/[kPa]	M_c	e_{r0}	λ	a/[kPa$^{0.5}$]	b	c
1000	1500	0.88	0.4	0.091	224	0.06	3.0
α	r_d	k_m	M_f	k	H_0/[kPa]	f_h	t/[m]
0.65	0.2	0.6	0.65	0.5	8500	2	0.1

4. Selection of engineering demand parameter

In order to study the effect of aftershocks on the fragility of the CFRD, a set of EDPs which can best reflect the cumulative damage effect of aftershocks on the CFRD needs to be selected. The EDPs are selected from among four parameters: horizontal deformation (X-displacement), vertical deformation (Y-Displacement), shear strain and DI. The PGA of the mainshock is increased from 0.2 g to 1 g at intervals of 0.1 g for each seismic sequence. It is universally known that the cases that aftershocks with larger PGA than mainshocks rarely occur in all earthquake records. Therefore, the relative intensity of aftershocks is scaled to 0.5, 0.7, 0.9 and 1. A total of 675 nonlinear dynamic time history analysis are performed and the dynamic responses of 675

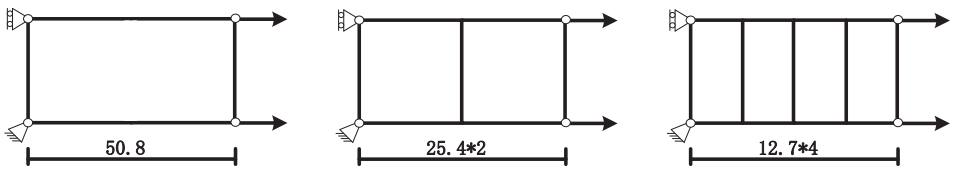

Fig. 2. Finite element meshes for mesh size sensitivity test.

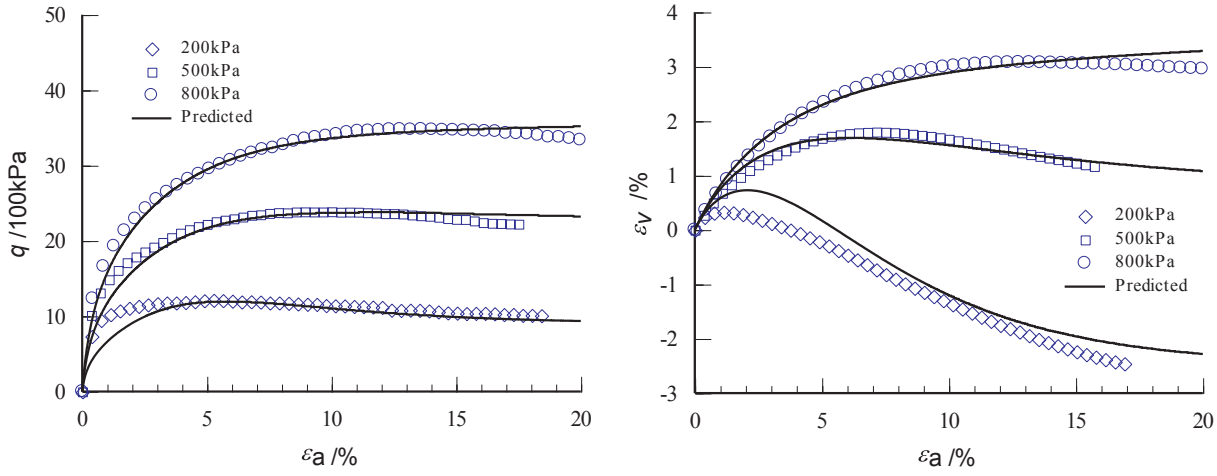

Fig. 4. Comparison of the model predictions and test results for the monotonic stress-axial strain and volumetric strain-axial strain relationships of the rockfill materials.

Table 4
The as-recorded mainshock-aftershock sequences used in this paper.

No.	Seismic sequence	Station name	Comp.	Date	Magnitude	PGA [g]	R_{jb} [km]
1	Northridge	Castaic-old ridge	90	1994-01-17	6.69	0.568	20.11
		Route		1994-01-17	5.93	0.138	22.23
2	Northridge	Rinaldi Receiving	318	1994-01-17	6.69	0.472	0
		Sta		1994-03-20	5.28	0.476	3.39
3	Chi-Chi	CHY035	E	1999-09-20	7.62	0.251	12.6
				1999-09-20	6.20	0.134	25.01
4	Chi-Chi	CHY024	E	1999-09-20	7.62	0.282	9.62
				1999-09-20	6.20	0.187	18.47
5	Cape mendocino/	1585 centerville	360	1992-04-25	7.00	0.480	26.5
	Petroli	Beach		1992-04-26	6.60	0.440	33.3
6	Cape mendocino/	1583 Fortuna fire	270	1992-04-25	7.00	0.334	32.7
	Petroli	Station		1992-04-26	6.60	0.396	47.1
7	Cape mendocino/	1586 Loleta fire	270	1992-04-25	7.00	0.400	35.1
	Petroli	Station		1992-04-26	6.60	0.350	45.3
8	Chalfant valley	Zack brothers	70	1986-07-20	5.80	0.272	6.07
		Ranch		1986-07-21	6.20	0.447	6.44
9	Coalinga	Pleasant valley	45	1983-05-02	6.40	0.300	7.69
		P.P		1983-07-22	5.80	0.575	13.16
10	Mammoth lake	Convict creek	90	1980-05-25	6.10	0.419	1.1
				1980-05-27	5.90	0.266	6.44
11	Mammoth lake	54,099 convict creek	180	1980-05-25	6.10	0.400	9.1
				1980-05-27	5.90	0.500	3.4
12	Whittier narrows	24,400 obregon park	360	1987-10-01	6.10	0.429	14.2
				1987-10-04	5.30	0.315	16.3
13	Whittier narrows	24,402 eaton canyon	0	1987-10-01	6.10	0.305	19.4
		Park		1987-10-04	5.30	0.271	18.2
14	Kozani	ITSAK	0	1995-05-13	6.10	0.215	19.5
				1995-05-17	5.30	0.129	12.1
15	Imperial valley	El centro array #5	140	1979-10-15	6.53	0.520	1.76
				1979-10-15	5.01	0.240	8.56

groups of CFRD are computed.

The EDPs of the CFRD under mainshock-aftershock sequence are compared with the corresponding EDPs of the CFRD under a single mainchock, through the scatter plot. Fig. 5 shows the case which mainshock and aftershock have the same PGA (PGA_{ms} = 0.2 g, PGA_{as} = 0.2 g). It can be seen from Fig. 5 that the shear strain and DI of the CFRD due to aftershocks do not increase significantly compared with mainshocks in most seismic sequences. Moreover, in some cases, the X-displacement of the CFRD under the action of a seismic sequence is smaller than the X-displacement caused by a single mainshock. Similar results have been found in some studies [8,31,43]. This phenomenon may be due to the polarity of the ground motions (e.g. mainshock is in the opposite direction as the aftershock). However, the Y-Displacements of the CFRD are greatly increased by aftershocks in all 15 seismic sequence sequences. Fig. 6 shows the case in which the aftershock has a smaller PGA than the mainshock. As the relative intensity of aftershock decreases, the cumulative effect of aftershocks on shear strain, DI and X-Displacement of the CFRD decreases significantly. In most cases, these three EDPs of the CFRD under the action of seismic sequences changed minimally compared with those under the action of a single mainshock. However, closer attention to the Y-Displacements of the CFRD shows that the arrival of aftershocks causes a more apparent increase to vertical deformation.

The same conclusion can be obtained from other cases of relative intensities, thus the other cases are not presented in this paper due to limited space. The above conclusions suggest that aftershocks contribute most to vertical deformation of the CFRD. It should be noted that vertical deformation has always been a key EDP used by scholars to

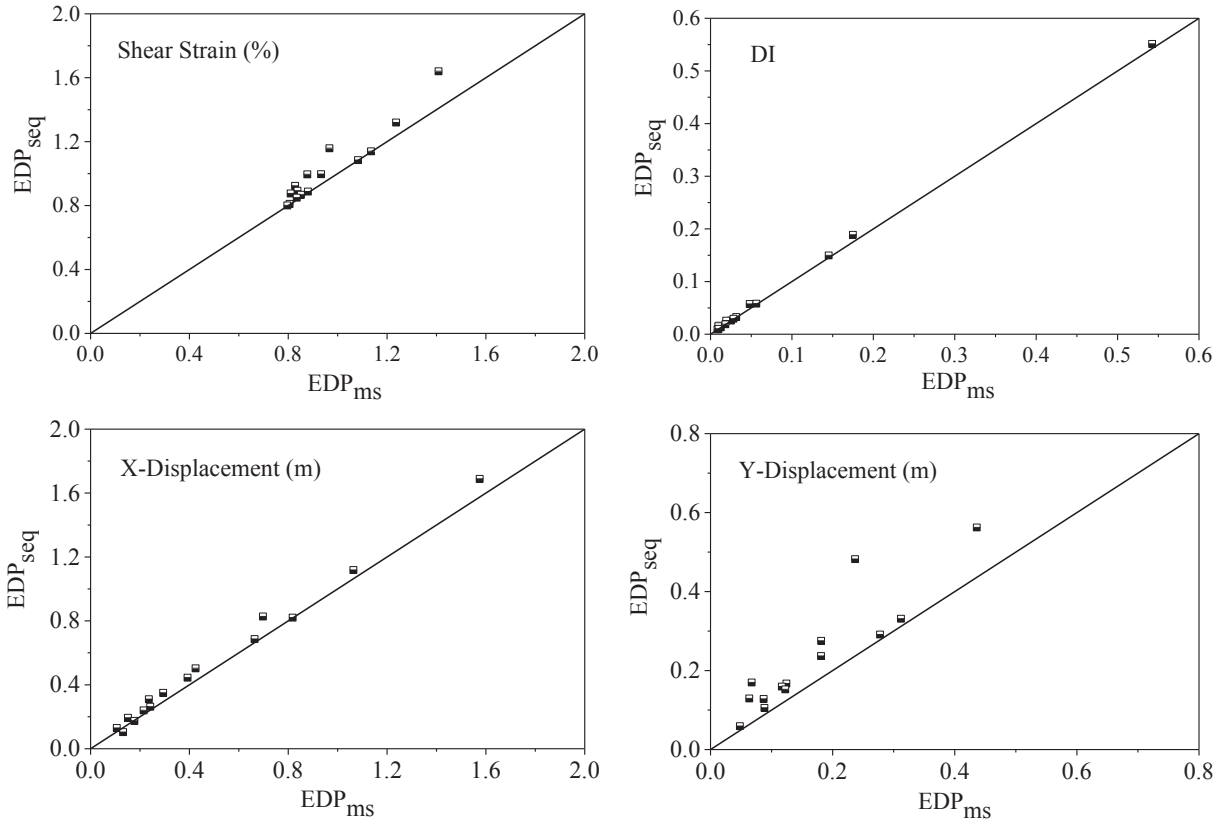

Fig. 5. Comparison of dam EDPs under mainshock-aftershock sequence (PGA_{ms} = 0.2 g, PGA_{as} = 0.2 g) (EDP_{seq}) vs. single mainshock (EDP_{ms}).

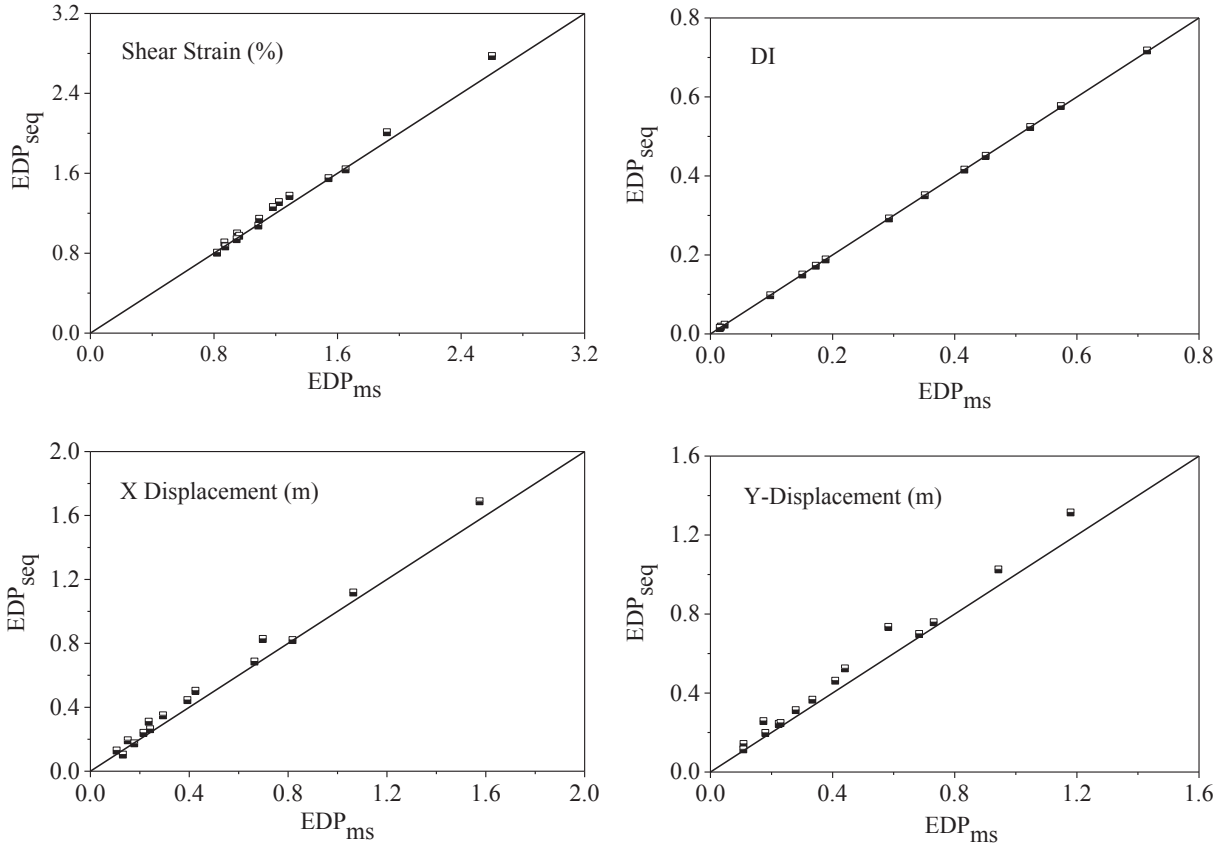

Fig. 6. Comparison of dam EDPs under mainshock-aftershock sequence (PGA_{ms} = 0.4 g, PGA_{as} = 0.2 g) (EDP_{seq}) vs. single mainshock (EDP_{ms}).

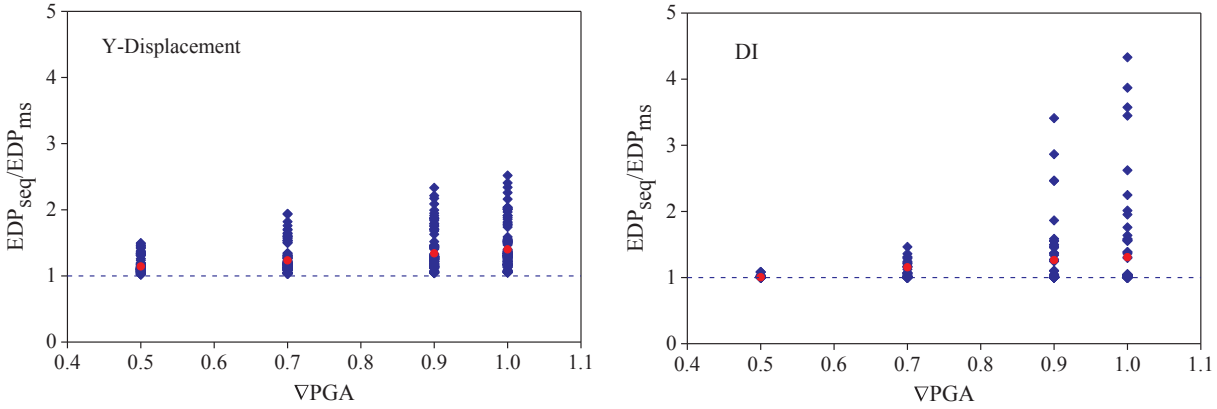

Fig. 7. Scatter plot of EDP_{seq}/EDP_{ms} vs. ∇PGA.

study the seismic performance of the CFRDs [25,26,44]. Taking the above contents into consideration, vertical deformation is selected as the EDP to study the fragility of the CFRD subjected to seismic sequences. In practice, the concrete face slabs play a critical role in the seepage control system of the CFRD, and damages to the concrete face slabs directly affect the safety of the dam. Consequently, many scholars [24,25,27] regard face slab damage as a key index to evaluate the safety of the CFRD when analyzing the dynamic response of the CFRD. Thus, the face slabs DI is also used as the EDP for fragility analysis in this paper.

Fig. 7 shows the scatter plot of EDP_{seq}/EDP_{ms} versus ∇PGA. The red dots represent the mean of EDP_{seq}/EDP_{ms} for each ∇PGA. The figure shows that when ∇PGA increases from 0.5 to 1.0, the mean EDP_{seq}/EDP_{ms} for vertical deformation changes from 1.143 to 1.401, and the mean EDP_{seq}/EDP_{ms} for the DI changes from 1.01 to 1.308. Thus, as the relative intensity of the aftershock increases, the potential damage caused by aftershocks (e.g. vertical deformation and DI) increases. However the effect of aftershocks on the CFRD vertical deformation is greater than for the DI.

5. Fragility analysis

In this study, the failure grade classification method based on vertical deformation and DI for the high CFRDs [25,26] is adopted. The classification criteria are listed in Tables 5 and 6. The fragility probability curves of the high CFRD for vertical deformation and DI are obtained via the MSA method. The fragility of the CFRD subjected to ground motions is analyzed for different limit states and relative intensities of the aftershock. Fig. 8 shows the fragility curves of the CFRD when the vertical deformation is set as the EDP. Seen from Fig. 8(a), the probability of the dam sustaining minor damage is 28.55% under the action of a single earthquake event with PGA of 0.3 g, and moderate and severe damage is unlikely to occur. When PGA is 0.7 g, the dam is very prone to minor damage, and the probabilities of moderate damage and severe damage are 44.56% and 18.85%, respectively. The probability of minor damage to the dam is over 90% and the probability of severe damage to the dam is close to 50% when the PGA reaches 1 g. Fig. 8(b–d) shows that the fragility curves of mainshock-aftershock sequences are all above the fragility curves of the single mainshocks

Table 5
The limit state partitions in this study based on vertical deformation of the CFRD.

Limit state	Vertical deformation	Failure grade
LS1	0.4 m	Minor
LS2	0.8 m	Moderate
LS3	1.2 m	Severe

Table 6
The limit state partitions in this study based on DI of the CFRD.

Limit state	DI	Failure grade
LS1	0.03	Minor
LS2	0.15	Noderate
LS3	0.45	Severe

and that the probability of the dam reaching various limit states increases when aftershocks are considered. Moreover, the probability of the dam reaching the limit state increases with direct proportionality to the relative intensity of aftershock. Taking PGA_{ms} = 0.7 as an example, when the relative intensity ∇PGA = 1, the seismic sequence increases the probability of the dam reaching LS1, LS2 and LS3 by 19.45%, 39.8% and 75.65%, respectively, compared to when only a single mainshock is inputted. When the relative intensity ∇PGA = 0.9, the probability of the dam reaching LS1, LS2 and LS3 increases by 16.35%, 30.09% and 58.78%; when the relative intensity ∇PGA = 0.7, the probability of the dam reaching LS1, LS2 and LS3 increases by 13.1%, 20.19% and 36.13%; when the relative intensity ∇PGA = 0.5, the probability of the dam reaching LS1, LS2 and LS3 increases by 5.89%, 6.93% and 24.88%. These dramatic surges in damage probability suggest that aftershocks contribute considerably to the high CFRD damage from the perspective of vertical deformation.

In addition to vertical deformation, the fragility analysis of the CFRD based on DI is also performed. As shown in Fig. 9, when using DI as the EDP, the dam appears to reach the limit states at a much quicker rate than with vertical deformation as the EDP. The difference in the rate may be due the higher sensitivity of DI to ground motions than vertical deformation. Similarly, taking PGA_{ms} = 0.6 as an example: when the relative intensity ∇PGA = 1, the seismic sequence increases the probability of the dam reaching LS1, LS2 and LS3 by 2.76%, 11.26% and 31.1% compared to when only a single mainshock is inputted; when the relative intensity ∇PGA = 0.9, the probability of the dam reaching LS1, LS2 and LS3 increases by 1.43%, 8.59% and 22.07%; when the relative intensity ∇PGA = 0.7, the probability of the dam reaching LS1, LS2 and LS3 increases by 0.63%, 5.8% and 15.33%; when the relative intensity ∇PGA = 0.5, the probability of the dam reaching LS1, LS2 and LS3 increases by 0.4%, 2.29% and 8.76%. The above results demonstrate that the effect of aftershocks on the fragility of the CFRD is not as pronounced as when vertical deformation is used as the EDP (Fig. 8).

6. Conclusions

This paper studies the effect of aftershocks on the fragility of the high CFRDs with a 200 m high CFRD as an example. 15 as-recorded mainshock-aftershock sequences are selected from the earthquake

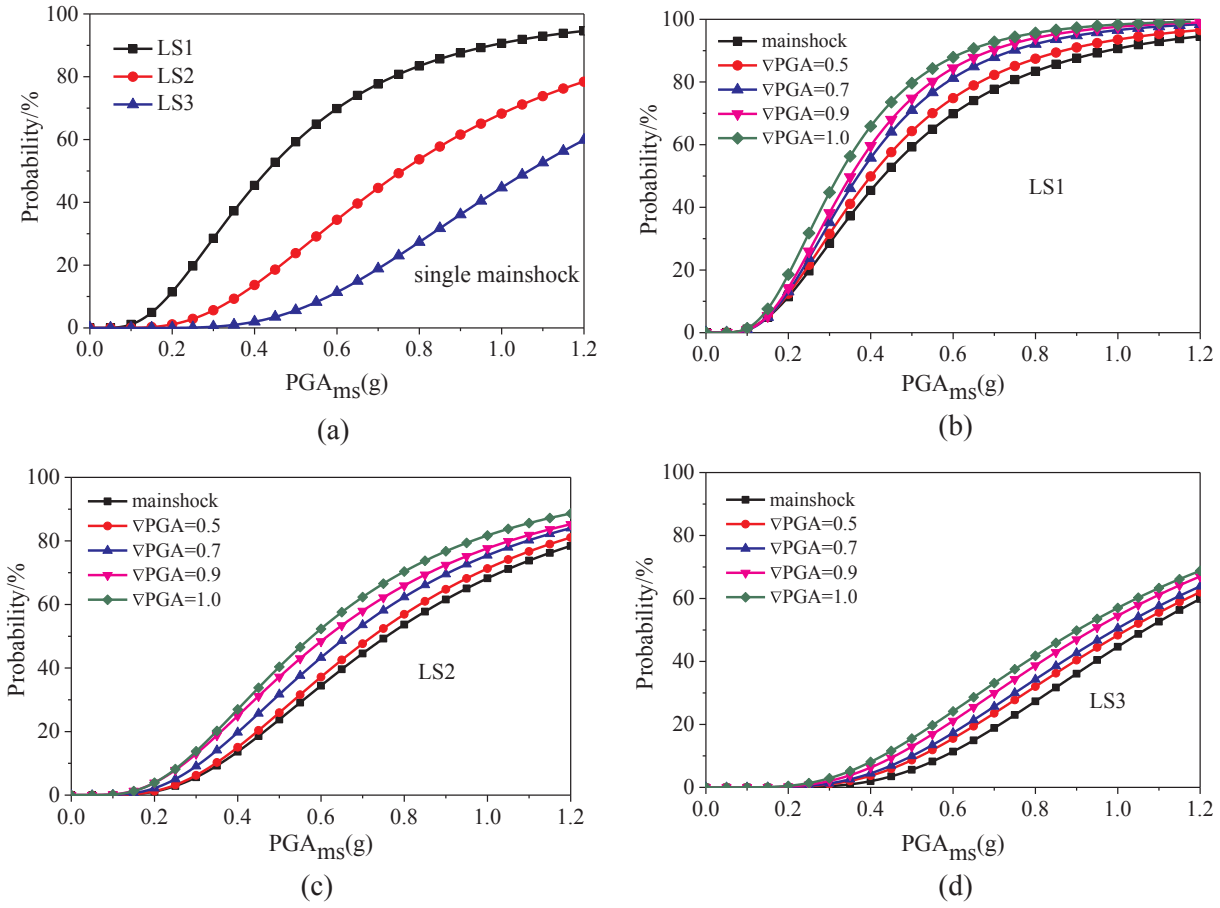

Fig. 8. Fragility curves of CFRD under different seismic conditions and different limit states with vertical deformation.

database [29,30] to enable a series of nonlinear dynamic time history analyses of the high CFRD based on four EDPs (X-displacement, Y-displacement, shear strain and DI). The EDP which can best reflect the cumulative damage effect of aftershocks on the CFRD is selected. Then the fragility analysis of the CFRD under seismic sequences is carried out. The following conclusions can be drawn:

(1) The vertical deformation is the most appropriate and effective EDP that can be used to study the cumulative damage caused by aftershocks to the high CFRD. The horizontal deformations of the CFRD may increase or decrease after the aftershocks.
(2) Compared with the action of a single mainshock, seismic sequences can increase the probability of the high CFRD plastic failure. Regardless of whether DI or vertical deformation is used as the EDP, this conclusion is applicable. The presence of aftershocks increases the probability of the CFRD towards reaching the ultimate state, and further the amplification as the state evolves from LS1 towards LS3. In the case of earthquake intensities listed in Section 5, when vertical deformation and DI are used as EDPs, the seismic sequence (including aftershocks) increases the probability of the CFRD reaching LS3 increases by 75.65% and 31.1%, respectively, when compared to the baseline case of a single mainshock. However, for LS1, the probability only increases by 19.45% and 2.76%.
(3) Aftershock contributes more to the fragility of the high CFRD based on vertical deformation than those based on DI. In addition, the damage probability of dam based on DI is higher than that based on vertical deformation under the same combination of mainshock-aftershock sequences.
(4) From the selection of EDP to the fragility analysis, the fragility of high CFRDs under mainshock-aftershock sequences are systematically analyzed. The damage level of the high CFRDs subjected to mainshock-aftershock sequences with a specific intensity combination is presented. The research content of this paper can serve as a valuable reference for future research efforts in analyzing the fragility of the CFRDs under mainshock-aftershock sequences.

It is noteworthy that only 15 as-recorded mainshock-aftershock sequences are selected and there are no analyses of other ground motion intensity metrics except PGA in this paper. The characteristics between artificial ground motions and as-recorded ground motions are different. Future research should focus on further understanding the structure of mainshock-aftershock sequences and the relationship between other intensity measures and EDPs.

Declaration of Competing Interest

We declare that we do not have any commercial or associative interest that represents a conflict of interest in connection with the work submitted.

Acknowledgements

This work was supported by National Key R&D Program of China (2017YFC0404904), the National Natural Science Foundation of China (Grant Nos. 51979026 and 51779034) and the Postdoctoral Innovative Talent Support Program of China (Grant No. BX20190057). These financial supports are gratefully acknowledged.

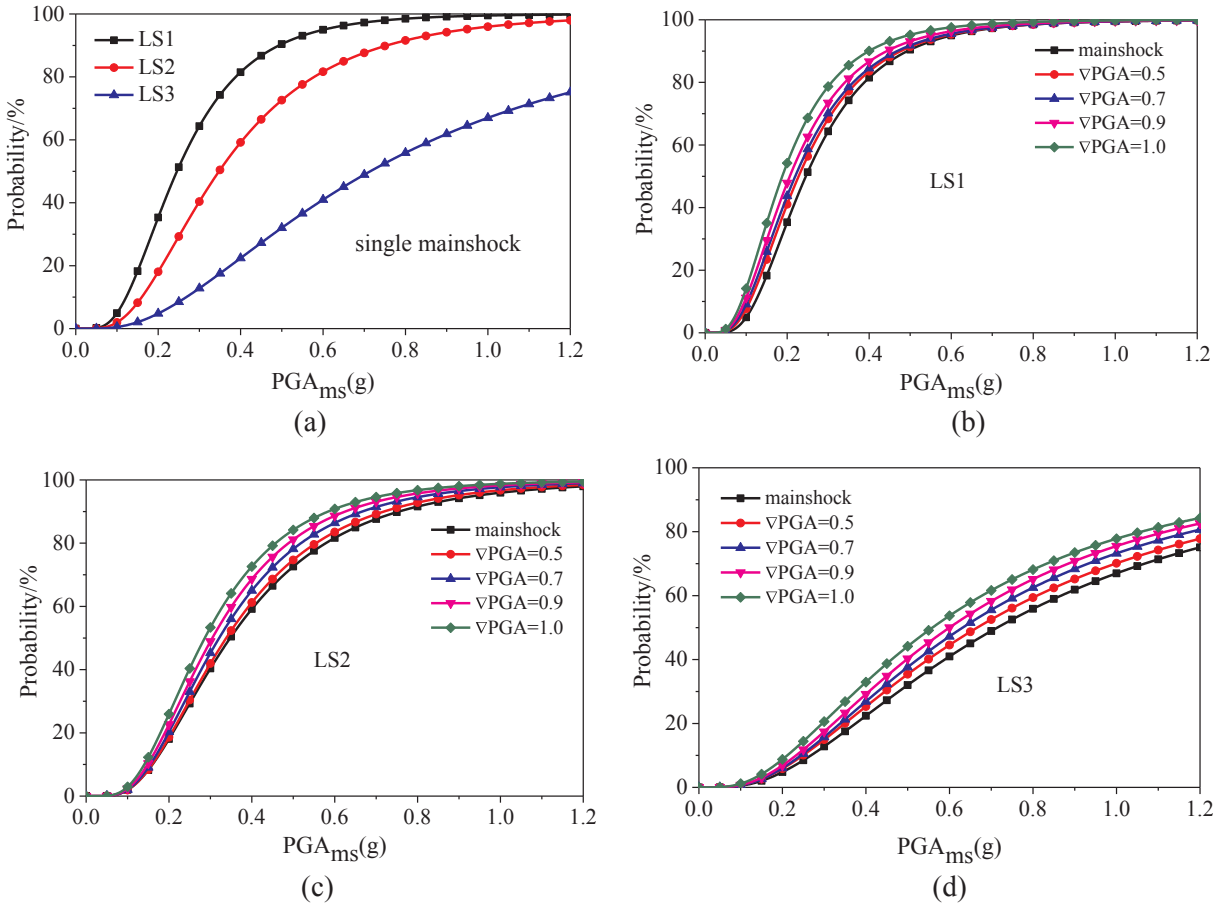

Fig. 9. Fragility curves of CFRD under different seismic conditions and different limit states with DI.

References

[1] Alliard PM. Mainshocks and aftershocks sequences database 2006.
[2] Sichuan earthquake 2008. Available from: http://en.wikipedia.org/wiki/2008_Sichuan_earthquakeS.
[3] Kyoshin-Net. National Research Institute for Earth Science and Disaster Prevention 2009, Available at http://www.k-net.bosai.go.jp/.
[4] China Earthquake Networks Center 2008. Available at http://www.csndmc.ac.cn/newweb/.
[5] Chinese S. Specifications for seismic design of hydraulic structures. Beijing: Chinese Electric Power Press; 2001.
[6] Alliard P, Leger P. Earthquake safety evaluation of gravity dams considering aftershocks and reduced drainage efficiency. J Eng Mech 2008;134(1):12–22.
[7] Zhang SR, Wang GH, Sa WQ. Damage evaluation of concrete gravity dams under mainshock-aftershock seismic sequences. Soil Dyn Earthq Eng 2013;50:16–27.
[8] Wang GH, Wang YX, Lu WB. Damage demand assessment of mainshock-damaged concrete gravity dams subjected to aftershocks. Soil Dynd Earthq Eng 2017;98:141–54.
[9] Pang R, Xu B, Zhang X, Zhou Y, Kong XJ. Seismic performance investigation of high CFRDs subjected to mainshock-aftershock sequences. Soil Dynd Earthq Eng 2019;116:82–5.
[10] Hariri-Ardebili MA, Saouma VE. Probabilistic seismic demand model and optimal intensity measure for concrete dams. Struct Saf 2016;59:67–85.
[11] Hariri-Ardebili MA, Saouma VE. Collapse fragility curves for concrete dams: comprehensive study. J Struct Eng 2016;142(10):04016075.
[12] Hariri-Ardebili MA, Saouma VE. Seismic fragility analysis of concrete dams: a state-of-the-art review. Eng Struct 2016;128:374–99.
[13] Wang JT, Zhang MX, Jin AY, Zhang CH. Seismic fragility of arch dams based on damage analysis. Soil Dynd Earthq Eng 2018;109:58–68.
[14] Gasser C, Goldgruber M, Bucher C. Seismic fragility curves of an arch dam with special regard to ultimate limit state. ASCE-ASME J Risk and Uncert in Engrg Sys Part B Mech Engrg 2019;5(4). https://doi.org/10.1115/1.4044151.
[15] Gasser C. Contributions to reliability assessment of engineering structures with special consideration of the seismic safety of an arch dam. Ph.D. Thesis. VCE Vienna Consulting Engineers ZT GmbH, Austria 2019. https://doi.org/10.13140/RG.2.2.14069.63205.
[16] Tekie PB, Ellingwood BR. Seismic fragility assessment of concrete gravity dams. Earthq Eng Struct Dyn 2003;32(14):2221–40.
[17] Bernier C, Padgett JE, Proulx J, Paultre P. Seismic fragility of concrete gravity dams with spatial variation of angle of friction: case study. J Struct Eng 2016;142(5):05015002.
[18] Bernier C, Monteiro R, Paultre P. Using the conditional spectrum method for improved fragility assessment of concrete gravity dams in eastern Canada. Earthq Spectra 2016;32(3):1449–68.
[19] Yazdani Y, Alembagheri M. Seismic vulnerability of gravity dams in near-fault areas. Soil Dynd Earthq Eng 2017;102:15–24.
[20] Sotoudeh MA, Ghaemian M, Moghadam AS. Determination of limit-states for near-fault seismic fragility assessment of concrete gravity dams. Sci Iran 2019;26(3):1135–55.
[21] Moradloo J, Naserasadi K, Zamani H. Seismic fragility evaluation of arch concrete dams through nonlinear incremental analysis using smeared crack model. Struct Eng Mech 2018;68(6):747–60.
[22] Pang R, Xu B, Zou DG, Kong XJ. Seismic performance assessment of high CFRDs based on fragility analysis. Sci China Technol Sci 2019;62(4):635–48.
[23] Xu B, Pang R, Zhou Y. Verification of stochastic seismic analysis method and seismic performance evaluation based on multi-indices for high CFRDs. Eng Geol 2020;264:105412. https://doi.org/10.1016/j.enggeo.2019.105412.
[24] Pang R, Xu B, Kong XJ. Seismic fragility for high CFRDs based on deformation and damage index through incremental dynamic analysis. Soil Dyn Earthq Eng 2018;104:432–6.
[25] Pang R, Xu B, Zou DG, Kong XJ. Stochastic seismic performance assessment of high CFRDs based on generalized probability density evolution method. Comput Geotech 2018;97:233–45.
[26] Xu B, Zou DG, Kong XJ, Hu ZQ, Zhou Y. Dynamic damage evaluation on the slabs of the concrete faced rockfill dam with the plastic-damage model. Comput Geotech 2015;65(4):258–65.
[27] Xu B, Wang XL, Pang R, Zhou Y. Influence of strong motion duration on the seismic performance of high CFRDs based on elastoplastic analysis. Soil Dyn Earthq Eng 2018;114:438–47.
[28] Pang R, Xu B, Kong XJ, Zhou Y, Zou DG. Seismic performance evaluation of high CFRD slopes subjected to near-fault ground motions based on generalized probability density evolution method. Eng Geol 2018;246:391–401.
[29] PEER Strong Motion Database: http://peer.berkeley.edu.
[30] Cosmos Virtual Data Center: http://strongmotioncenter.org.
[31] Wen WP, Zhai CH, Ji DF, Li S, Xie LL. Framework for the vulnerability assessment of structure under mainshock-aftershock sequences. Soil Dyn Earthq Eng 2017;101:41–52.
[32] Baker JW. Efficient analytical fragility function fitting using dynamic structural analysis. Earthq Spectra 2013;31(1):579–99.

[33] Westergaard HM. Water pressures on dams during earthquakes. Translator 1933;98:418–33.
[34] Qu YQ, Zou DG, Kong XJ, Xu B. A novel interface element with asymmetric nodes and its application on concrete-faced rockfill dam. Comput Geotech 2017;85:103–16.
[35] Liu JB, Lu YD. A direct method for analysis of dynamic soil-structure interaction. China Civil Eng J 1998;31(3):55–64. [in Chinese].
[36] Lee J, Fenves GL. A plastic-damage concrete model for earthquake analysis of dams. Earthq Eng Struct Dyn 1998;27(9):937–56.
[37] Lee J, Fenves GL. Plastic-damage model for cyclic loading of concrete structures. J Eng Mech 1998;124(8):892–900.
[38] Wen LF, Chai JR, Xu ZG, Qin Y, Li YL. Comparative and numerical analyses of response of concrete cutoff walls of earthen dams on alluvium foundations. J Geotech Geoenviron Eng 2019;145(10):04019069.
[39] Atta M, Abd-Elhady AA, Abu-Sinna A, Sallam HEM. Prediction of failure stages for double lap joints using finite element analysis and artificial neural networks. Eng Fail Anal 2019;97:242–57.
[40] Zou DG, Xu B, Kong XJ, Liu HB, Zhou Y. Numerical simulation of the seismic response of the Zipingpu concrete face rockfill dam during the Wenchuan earthquake based on a generalized plasticity model. Comput Geotech 2013;49:111–22.
[41] Kong XJ, Liu JM, Zou DG. Numerical simulation of the separation between concrete face slabs and cushion layer of Zipingpu dam during the Wenchuan earthquake. Sci China Technol Sci 2016;56(4):531–9.
[42] Song RQ, Li Y, van de Lindt JW. Impact of earthquake ground motion characteristics on collapse risk of post-mainshock buildings considering aftershocks. Eng Struct 2014;81:349–61.
[43] Ruiz-Garcia J, Aguilar JD. Aftershock seismic assessment taking into account post-mainshock residual drifts. Earthq Eng Struct Dyn 2015;44(9):1391–407.
[44] Xu B, Zhou Y, Zhou CG, Kong XJ, Zou DG. Dynamic responses of concrete-faced rockfill dam due to different seismic motion input methods. Int J Distrib Sens N 2018;14(10). 1550147718804687.